Welding in the World (2018) 62:675–682
https://doi.org/10.1007/s40194-018-0585-7

RESEARCH PAPER

Joining of 3D-printed AlSi10Mg by friction stir welding

Z. Du[1] · M. J. Tan[1] · H. Chen[2] · G. Bi[2] · C. K. Chua[1]

Received: 14 July 2017 / Accepted: 15 March 2018 / Published online: 28 March 2018

Abstract
Friction stir welding is a solid-state welding technology capable of joining metal parts without melting. The microstructure of the material evolved during the process from columnar grain along the thermal gradient in the melt pool to fine equiaxed grains. A significant decrease in microhardness in the stir zone was observed with the lowest hardness at approximately 3 mm from the weld centre. The decrease in the microhardness is mainly attributed to the dissolution of hardening precipitates in the aluminium matrix. Defects in the weld were observed due to insufficient heat input. Heat input could be increased with the increase in rotational speed of the welding tool, with some improvements in strength.

Keywords Welding · AlSi10Mg · Joining · Friction stir welding · Selective laser melting · Additive manufacturing

1 Introduction

Selective laser melting (SLM) is a powder bed fusion, an additive manufacturing technique using a laser beam melting powder layer by layer. With the aid of a CAD computer technique, a three-dimensional virtual object could be sliced into many layers and sent to the SLM for layerwise production. A thin layer of powder is laid onto the building platform before the laser melts the powder. The laser melts the powder to form a solidified part. The laser will continue to trace and melt the cross-sectional area of the layer. After the laser exposure, the platform is lowered by a layer thickness specified by the user. A new layer of powder is spread across the platform before the laser shines the cross-section area of the next layer. The process repeats and continues until the desired build part is completed. SLM is capable of producing quality parts with dimensional accuracy, superior mechanical properties and complex geometry. However, the SLM has a limited capacity to its build volume. Moreover, residual stresses and thermal distortion are more evident when printing large parts. Therefore, welding presents a viable solution to joint SLM-printed parts together.

Friction stir welding (FSW) is the solid-state joining technique consisting of a non-consumable rotating tool, a threaded pin and shoulder, being inserted into the abutting edges of the workpiece and traversing along the weld direction. During the process, friction between the rotating tool and the workpiece soften the workpiece permitting plastic deformation and dynamic recrystallisation process to occur, hence, welding the workpiece without melting. The intense plastic deformation together with the elevated temperature during the process results in fine equiaxed recrystallised grains in the nugget region [1–3].

The union of the two different processes will enable the fabrication and the joining of parts with complex features. The scope of this study is to join aluminium parts printed via SLM using FSW to weld the parts together. The objective of this study is to examine the mechanical properties and the microstructure evolution of the welded butt joint.

This article is part of the collection Welding, Additive Manufacturing and Associated NDT.

✉ Z. Du
ZDU003@ntu.edu.sg

M. J. Tan
mmjtan@ntu.edu.sg

H. Chen
hcchen@simtech.a-star.edu.sg

G. Bi
gjbi@simtech.a-star.edu.sg

C. K. Chua
mckchua@ntu.edu.sg

[1] Singapore Centre for 3D Printing, School of Mechanical & Aerospace Engineering, Nanyang Technological University, 50 Nanyang Avenue, Singapore 639798, Singapore

[2] Singapore Institute of Manufacturing Technology (SIMTech), 73 Nanyang Dr, Singapore 637662, Singapore

2 Methodology

Gas atomised spherical AlSi10Mg aluminium alloy from TLS Technik GmbH Co. with normally distributed particle size ranging from 20 to 63 μm was used. The *SLM 250HL*, *Germany*, equipped with a 400 W YLR-Faser-Laser, a Gaussian laser beam profile laser and spot size of 80 μm was used in this study. Rectangular block measuring 100 × 60 × 10 mm was fabricated via SLM with chessboard scanning strategy to provide even heating and reduction in thermal distortion of the build parts [4]. The SLM fabrication parameters are tabulated in Table 1.

FSW was performed with a threaded conical probe with three flats. The probe has a length of 6 mm and a base diameter of 7 mm. The diameter of the tool shoulder is 15 mm. A single pass weld was performed on the workpiece to join the two parts together.

Metallographic samples were sectioned from the cross-section of the weld and mechanically polished using conventional methods before being examined with the field emission scanning electron microscope (FESEM), *Joel JSM-7600F*, *USA*, equipped with electron backscatter diffraction (EBSD), *Oxford Instruments*, *USA*. EBSD was used to map the misorientation profile using Channel 5 software by HKL Technology with a step size of 0.2–0.5 μm. Keller's reagent was used to etch the samples for optical microscopy. Vickers microhardness test was done along the cross-sectional surface of the sample using 50-g force loading.

Rectangular tensile coupons were cut out perpendicular to the weld. Tensile testing was conducted in accordance with ASTM E08-04 standards with a cross-head displacement speed of 1 mm min^{-1}. A minimum of three "I" shaped rectangular sub-sized samples with gauge length of 25 mm and width of the reduced section was 6 mm (Fig. 1). A fracture surface analysis was done using FESEM on the fractured surfaces.

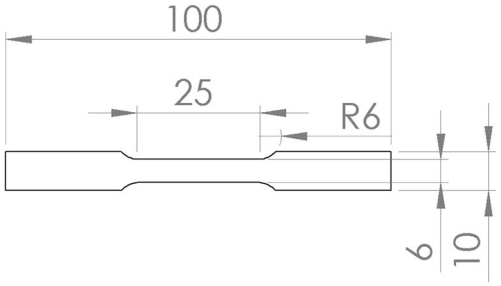

Fig. 1 Dimension used for the tensile specimen (units in mm)

3 Results and discussion

3.1 Grain structure evolution

Metallographic samples were observed under the FESEM. For samples from the SLM process, distinct melt pools were observed (Figs. 2a and 3a). Upon closer observation, alpha phase dendrites with Si-rich eutectic constituents were observed. The dendrites were also observed to grow in the direction thermal gradient of the melt pool. This could be explained by the formation of continuous melt track formed as laser shines and melts the layer of powder together with the previous layer while traversing along the melt track. The heat transfer is therefore in the radial direction from the centre to the edge of the melt pool. Rapid solidification occurs from the edge of the melt pool to the centre as shown from the direction of the Si-rich particles in the melt pool. The edge of the melt pool could be distinguished by very fine equiaxed grains forming a band at the edge of the melt pool.

On the other hand, fine equiaxed grains were observed in the weld nugget of the sample being welded via FSW (Figs. 2b and 3b). Si-rich particles were observed to have broken down during FSW and uniformly dispersed into the aluminium matrix. This is mainly attributed to the continuous dynamic recrystallisation caused by the introduction of continuous strain coupled with rapid

Table 1 Processing parameters for SLM and FSW

Material and processes	SLM	FSW-SLM with low heat input	FSW-SLM with high heat input	FSW-SLM with higher heat input
Laser power, P (watts)	350	350	350	350
Scanning speed, v (mm s^{-1})	1140	1140	1140	1140
Hatch spacing, h (mm)	0.17	0.17	0.17	0.17
Layer thickness, t (μm)	50	50	50	50
Energy density, E (10^{-9} J m^{-3})	36.12	36.12	36.12	36.12
Rotational speed (min^{-1})	–	1200	1200	1200
Travel speed (mm s^{-1})	–	3	1	1
Tilt angle (°)	–	2.5	2.5	4.5
Downward force (kN)	–	3.75 ± 0.2	1.57 ± 0.3	4.00 ± 0.2

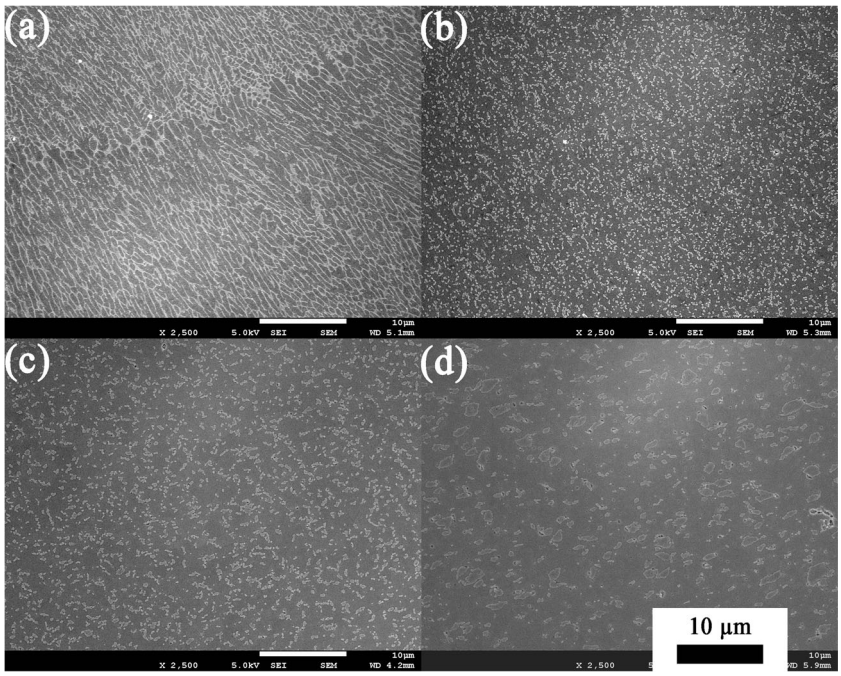

Fig. 2 Cross-section FESEM image of **a** AlSi10Mg, **b** FSWed AlSi10Mg (low heat input), **c** FSWed AlSi10Mg (high heat input) and **d** cross-section FESEM image of FSWed AlSi10Mg (higher heat input)

recovery and migration of sub-grain boundaries during friction stir welding [5, 6]. Samples with low heat input displayed finely dispersed Si-rich particles in the matrix. With the increase in the heat input, significant growth in the Si-rich particles were observed (Fig. 2c, d).

The grain sizes of the various samples were also examined (Table 2); significant grain refinement of the grains was observed after FSW. This is mainly attributed to dynamic recrystallisation coupled with intense plastic deformation that occurred during FSW.

Humphrey et al. suggested that grain growth after recrystallisation could be explained using Zenner pining effect [7]:

$$\frac{dR}{dt} = M(P - P_z) = M\left(\frac{\alpha\gamma_b}{R} - \frac{3F_{v\gamma b}}{2r}\right)$$

where M is the boundary mobility, P is the driving pressure from the curvature of the grain boundaries, P_z is the Zener pinning pressure, R is the radius of the grain, r is the radius

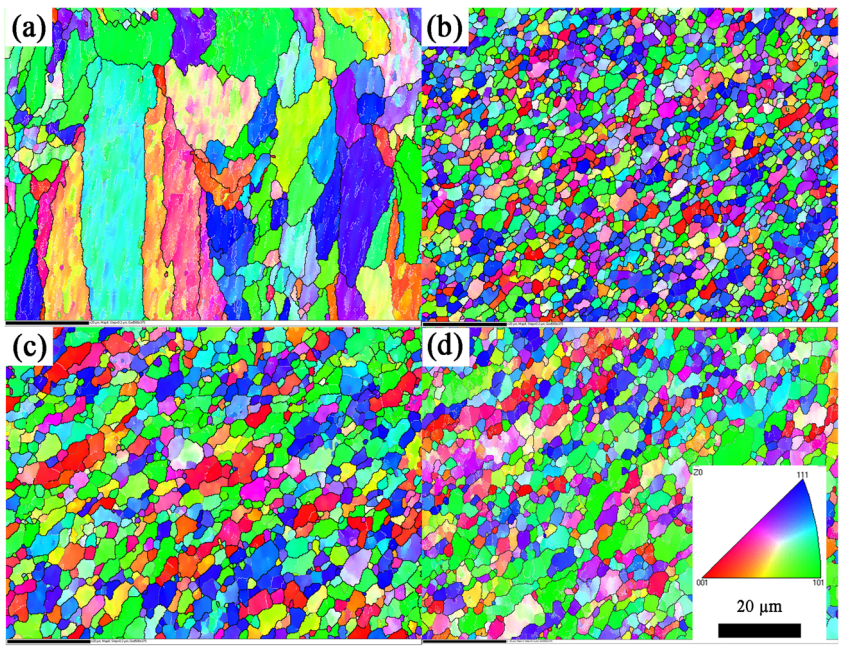

Fig. 3 EBSD mapping of **a** SLM AlSi10Mg, **b** FSWed AlSi10Mg with low heat input showing the grain structures, **c** FSWed AlSi10Mg with high heat input and **d** FSWed AlSi10Mg with higher heat input showing the grain structures. For the boundary misorientation, white lines: between 2° and 5°, grey lines: between 5° and 15°, black lines: > 15°. (The colour in this figure legend is explained in the web version of the article)

Table 2 Grain size

Material and process	AA6061-O	SLM AlSi10Mg	FSW-SLM with low heat input	FSW-SLM with high heat input	FSW-SLM with higher heat input
Grain size (μm)	23.25	6.0	2.1	2.8	2.76
Std. dev.	23.24	2.05	1.13	1.64	1.58

of the pinning particles, F_v is the volume fraction, α is a small geometric constant and γb is the boundary energy.

Comparing Fig. 3b and c, significant coarsening of the grains was observed and in agreement with the observation by Mishra et al. [8]. This is mainly attributed to the significant increase in the number of revolution made by the tool per unit length transverse. This resulted in an increase in heat input during the FSW process. It has reported that the heat generation can be increased via increasing the RPM [9, 10]. However, increasing the tilt angle does not have a significant effect on the grain refinement mechanism as observed in Fig. 3c, d. However, significant coarsening of the Si-rich particles was observed (Fig. 2d).

Misorientation of the grains in the weld nugget was examined in Fig. 4. A significant increase in the high-angle boundary was observed in the samples after FSW (Table 3). This is mainly attributed the intense plastic deformation and stirring of the material in the stir zone. It was also observed that an increase in heat input via increasing the RPM to traverse speed ratio resulted in the decrease in the high-angle boundaries present in the weld nugget. However, increasing the tilt angle has no significant effect on the misorientation of the material. During FSW, the material underwent massive strain coupling with rapid recovery at the grain/sub-grain boundaries due to the rotating motion. This stored energy drove the dynamic recovery and recrystallisation processes. Further grain deformation led to the gradual lattice rotation associated with sliding [11, 12] and grains with high-angle boundaries. By applying the continuously rotating motion, grains with low-angle boundaries in the base material were transformed into grains with high-angle boundaries in the stir zone [3].

3.2 Microhardness

The microhardness of the SLM printed samples was observed to be higher than that of AA6061-O (Table 4). This could be mainly attributed to the SLM process. During SLM, the material experiences rapid melting and cooling process. The rapid solidification process produces very fine grains compared to conventionally fabricated AA6061-O samples as reported in previous studies [13, 14]. The presence of eutectic constituents could also have attributed to the increase in the hardness values of the SLM printed samples. Moreover, the severe thermal stresses leading to higher internal stresses and increased microhardness.

However, comparing AlSi10Mg samples before and after welding, there is a significant reduction in the hardness of the material in the weld nugget region (Fig. 5). This could be due the dissolution of hardening precipitated occurring during the thermal cycle of friction stir welding process as reported in another study [15]. High hardness in the SLM build could result from precipitation hardening by reheating by the laser. This agrees with the FSW results of aluminium by Sato et al. [16]. FSW samples with high heat input were observed to have a lower hardness as compared to FSW samples with low heat input. This could be mainly attributed to the larger

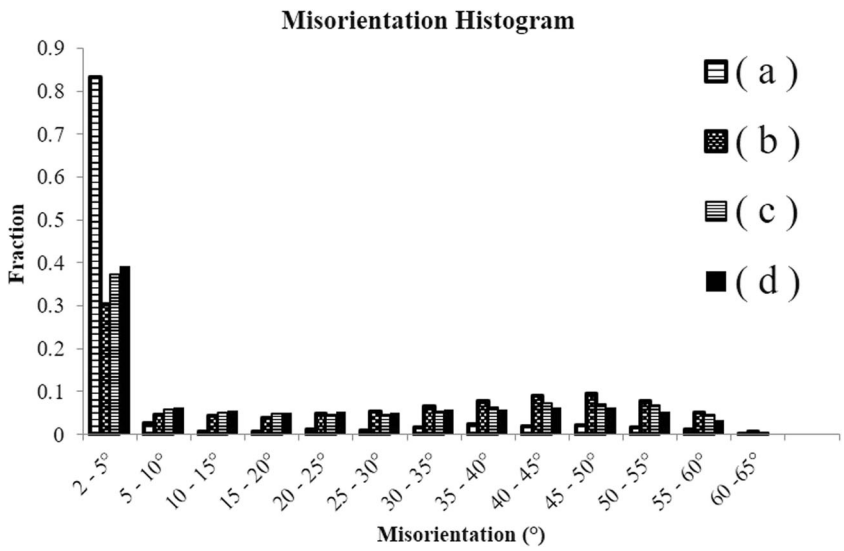

Fig. 4 Misorientation histogram distribution of grain/sub-grain misorientation angles for (a) SLM AlSi10Mg, (b) FSWed AlSi10Mg with low heat input, (c) FSWed AlSi10Mg with high heat input and (d) FSWed AlSi10Mg with higher heat input

Table 3 Summary of the misorientation distribution

Material and process	Mean grain misorientation	Fraction of high-angle grain boundaries (> 15°)	Fraction of low-angle grain boundaries (≤ 15°)		Number of samples
			(1–5°)	(1–15°)	
AlSi10Mg	7.07	0.14	0.83	0.86	99,709
FSW-SLM with low heat input	25.43	0.61	0.30	0.39	68,292
FSW-SLM with high heat input	21.80	0.52	0.37	0.48	53,217
FSW-SLM with higher heat input	20.04	0.49	0.39	0.51	56,795

Table 4 Microhardness result

Material and process	AA6061-O [17]	SLM AlSi10Mg	FSW-SLM with low heat input	FSW-SLM with high heat input	FSW-SLM with higher heat input
$Hv_{0.05}$	55 ± 3	127 ± 1	82 ± 1	65 ± 7	71 ± 1

grains as well as more dissolution of hardening precipitates due to higher heat input. There were no significant changes observed in the hardness values with the increase in tilt angle. However, it is observed that the gradient of the slope decreased with increasing heat input. This could be mainly attributed to the increase in the HAZ region with an increase in heat input.

3.3 Tensile test

Tensile testing was conducted perpendicular to the weld direction. The tensile test results were tabulated in Table 5 and Fig. 6. Comparing AlSi10Mg samples with and without

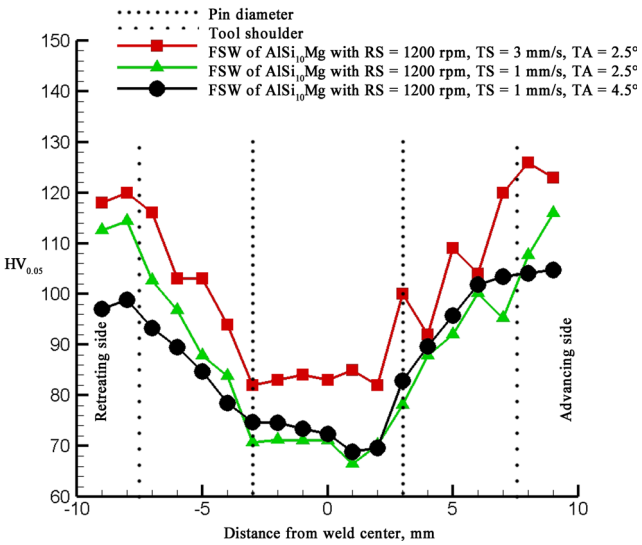

Fig. 5 Typical hardness curve across (a) FSWed AlSi10Mg with low heat input, (b) FSWed AlSi10Mg with high heat input and (c) FSWed AlSi10Mg with higher heat input

FSW, there is a significant reduction in the UTS from 476 to 173 MPa. From the stress-strain curve of the welded AlSi10Mg, a sudden drop in the stress followed by a short plastic deformation region could be attributed to the presence of welding defect.

Upon studying the cross-section of the weld, a faint zigzag-line crack was observed near the retreating side of the stir zone of the etched cross-sectional FSW (Fig. 7). This defect is also known as "lazy-S" defect as reported in another study [18]. The wavy contour of the crack follows the flow and deformation of the material during the weld and mainly attributed to the low heat input parameters. The material in the stir zone is unable to completely flow from the advancing side to the retreating side of the weld. The presence of the *lazy S* defect creates a weak region leading to a crack during the tensile test and poor mechanical properties. Therefore, increasing the heat input for FSW would be required to eliminate the defect. Heat input for FSW could be influenced by several FSW parameters. Several studies report the increase in rotational speed increased peak temperature [9, 19].

Heat input was increased by reducing the traverse speed of the FSW, and significant improvement in the tensile test result was observed as compared to samples with low heat input. This could only be mainly attributed to the increase in heat input allowing for better material flow during FSW. However, *lazy S* defect was still visible in the weld. During the FSW of AlSi10Mg with high heat input welding condition, flashing of the material were also observed. This is an indication of having too much heat input and the material in contact with the tool shoulder has softened significantly to be spun out of the shoulder. Thus, increasing the heat further via increasing the RPM to transverse speed ratio will only result in further softening of the material and more flashing defect. The tool will also sink deeper into the material due to the conservation of

Table 5 Tensile test properties

Material and process	Ultimate tensile test (MPa)	Yield strength (MPa)	Elongation (%)
AA6061-0 [21]	125	55	25
SLM AlSi10Mg	451 ± 10	265 ± 5	6.26 ± 1
FSW-SLM with low heat input	132 ± 5	110 ± 3	2.26 ± 0.5
FSW-SLM with high heat input	236 ± 5	128 ± 2	6.1 ± 1
FSW-SLM with higher heat input	240 ± 8	146 ± 5	8.32 ± 1

volume. Thus, to eliminate the *lazy S* defect, an increase in the tilt angle was used. This led to an increase in the downward force on the material. The increase in downward force forges and increases the material flow in the stir zone, creating a sound weld. From the tensile results, significant improvement in the ductility was observed, but no significant improvement in the tensile strength was observed.

Comparing AA6061-O with further (higher) heat input, significant improvement in the tensile yield strength and ultimate tensile strength were observed. This is many attributed to the grain refinement of FSW and could be explained using the Hall-Petch equation:

$$\sigma_y = \sigma_d + \frac{k_y}{\sqrt{d}}$$

where σy is the yield stress, σd is a material constant for the initial stress of dislocation movement, k_y is the strengthening coefficient and d is the average grain diameter.

The Orowan strengthening effect could have also taken place due to the presence of Si-rich particles. Extra energy is required for the dislocation planes to move past the obstacles. After moving past, it creates an Orowan loop around the particles increasing the resistance further [20].

3.4 Fractography

AlSi10Mg fracture without visible necking while fracture path was perpendicular to the direction of the applied force. Samples with low and high heat input fractured at the weld defect. Sample with higher heat input fractured in the middle of the weld. Significant necking was observed.

Observation of the fracture surface under the FESEM reviews the fracture mechanism that took place at the fracture site. Looking at fracture surface of the AlSi10Mg (Fig. 8a) and AlSi10Mg after FSW (Fig. 8b–d), dimples were observed at the fracture surfaces indicating ductile fracture mechanism. The dimples of the AlSi10Mg were relatively elongated as compared those of the FSWed samples. These could be due to the microstructure of the different material. The grains of the SLM samples are columnar and grow in the direction of the thermal gradient in the melt pool. Therefore, crack propagation could be along the grain boundaries resulting in elongated dimples. Voids were also observed on the fracture surface indicating the presence of small pores in the material.

On the other hand, the dimples of the FSW samples with low heat input were observed (Fig. 8b) to be relatively smaller and shallower, assembling the crack propagation along the *Lazy S* weld defect (Fig. 7c, d). For samples with high heat

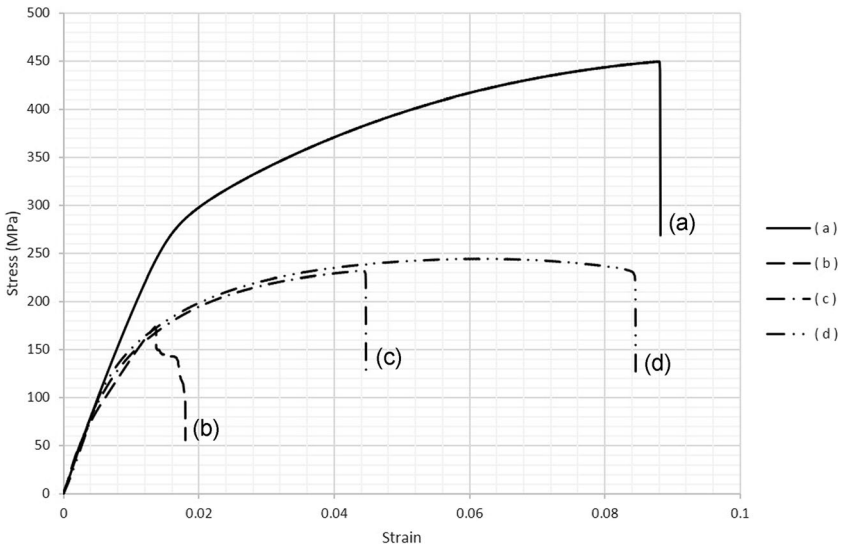

Fig. 6 Stress vs strain curve of the tensile test of (a) SLM AlSi10Mg, (b) FSWed AlSi10Mg with low heat input, (c) FSWed AlSi10Mg with high heat input and (d) FSWed AlSi10Mg with higher heat input

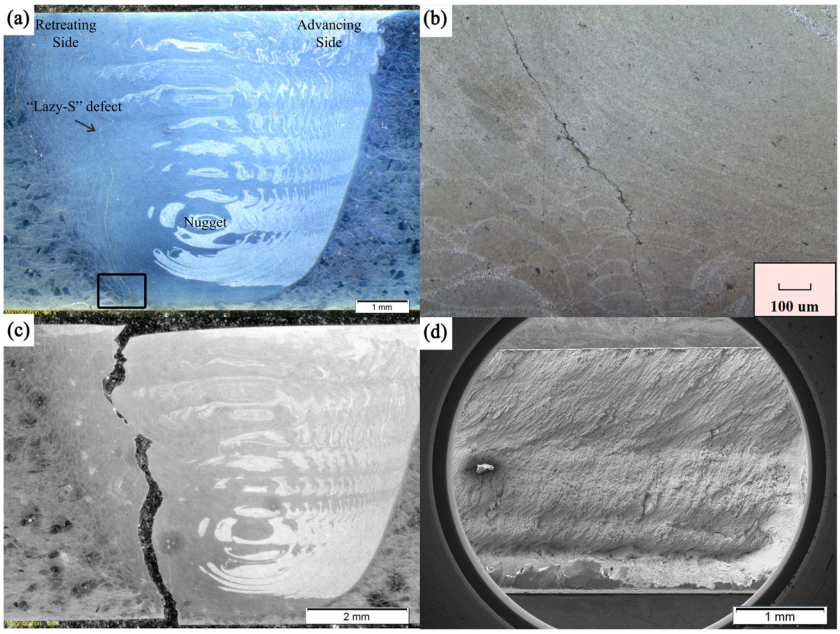

Fig. 7 Cross-section of FSW samples with **a** low heat input showing lazy S defect and **b** a close-up image of the "lazy-S" defect before and **c** after tensile test; **d** fracture surface of the tensile tested sample

input (Fig. 8c), deeper and larger dimples were observed. This could be due to better welding with higher heat input. However, the two pieces were not completely bonded together, and crack propagated along the *Lazy S* defect. As for the samples with higher heat input (Fig. 8d), a significant increase in depth and size of the dimple were observed indicating a very ductile fracture. During the tensile test, the slight plastic deformation phase as seen in the stress-strain curve could be due to the formation of microvoids at the grain boundaries. These voids continued to grow as the stress increases. The voids eventually merged and formed cracks that led to the failure of the material.

4 Conclusion

Butt welding using FSW has been successfully performed on SLM printed AlSi10Mg. Microstructure evolution of the material was observed from columnar grains along the thermal gradient to fine equiaxed grains in the stir zone due to the

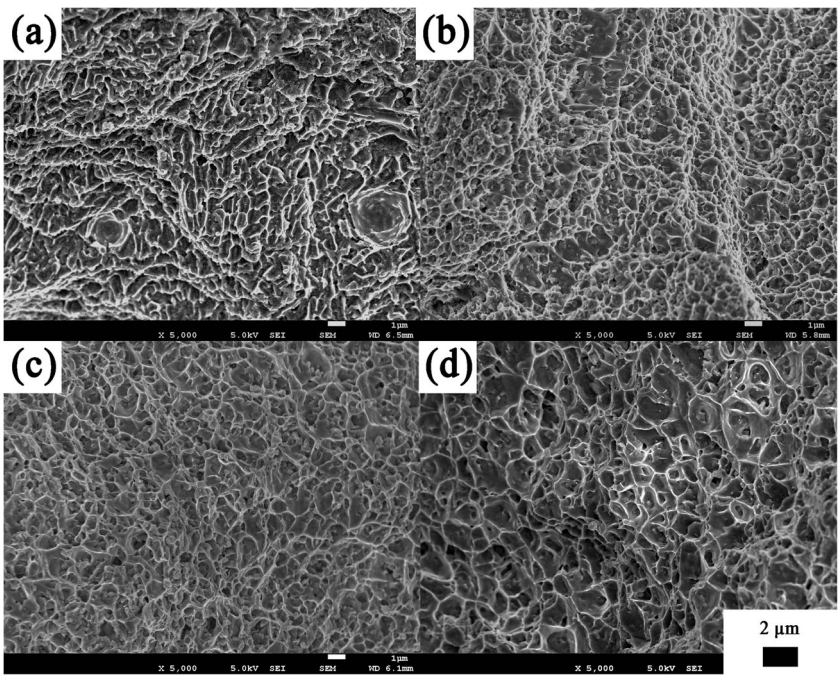

Fig. 8 FESEM image of the fracture site of **a** AlSi10Mg, **b** AlSi10Mg after FSW-SLM with low heat input, **c** AlSi10Mg after FSW-SLM with high heat input and **d** AlSi10Mg after FSW-SLM with higher heat input

continuous dynamic recrystallisation from the thermal cycle during FSW. A decrease in the microhardness in the stir zone was observed. The decrease in the microhardness is mainly attributed to the dissolution of hardening precipitates in the aluminium matrix. Defects on the weld were observed due to insufficient heat input. Heat input could be increased with the increase in rotational speed of the welding tool with some improvements in strength.

References

1. Rhodes CG, Mahoney MW, Bingel WH, Spurling RA, Bampton CC (1997) Effects of friction stir welding on microstructure of 7075 aluminum. Scr Mater 36(1):69–75
2. Liu G, Murr LE, Niou CS, McClure JC, Vega FR (1997) Microstructural aspects of the friction-stir welding of 6061-T6 aluminum. Scr Mater 37(3):355–361
3. Jata KV, Sankaran KK, Ruschau JJ (2000) Friction-stir welding effects on microstructure and fatigue of aluminum alloy 7050-T7451. Metall Mater Trans A 31(9):2181–2192
4. Jhabvala J, Boillat E, Antignac T, Glardon R (2010) On the effect of scanning strategies in the selective laser melting process. Virtual and Physical Prototyping 5(2):99–109
5. Su J-Q, Nelson TW, Sterling CJ (2005) Microstructure evolution during FSW/FSP of high strength aluminum alloys. Mater Sci Eng A 405(1–2):277–286
6. Fonda RW, Knipling KE, Bingert JF (2008) Microstructural evolution ahead of the tool in aluminum friction stir welds. Scr Mater 58(5):343–348
7. Humphreys F.J. and Hatherly M., Chapter 11 - Grain growth following recrystallization, ed. R.a.R.A.P.S. Edition). 2004, Oxford: Elsevier Ltd
8. Mishra R.S. and Ma Z.Y., Friction stir welding and processing. Materials Science and Engineering: R: Reports, 2005. 50(1–2): p. 1-78
9. Sato YS, Urata M, Kokawa H (2002) Parameters controlling microstructure and hardness during friction-stir welding of precipitation-hardenable aluminum alloy 6063. Metall Mater Trans A 33(3):625–635
10. Arbegast W.J., Hot deformation of aluminum alloys III, ed. Z. Jin, A. Beaudoin, T.A. Bieler, and B. Radhakrishnan. 2003: Wiley
11. Hales SJ, McNelley TR (1988) Microstructural evolution by continuous recrystallization in a superplastic Al-Mg alloy. Acta Metall 36(5):1229–1239
12. Gudmundsson H, Brooks D, Wert JA (1991) Mechanisms of continuous recrystallization in an Al □ Zr □ Si alloy. Acta Metall Mater 39(1):19–35
13. Du Z, Tan MJ, Guo JF, Wei J (2016) Aluminium-carbon nanotubes composites produced from friction stir processing and selective laser melting. Mater Werkst 47(5–6):539–548
14. Guo J.F., Liu J., Sun C.N., Maleksaeedi S., Bi G., Tan M.J., and Wei J., Effects of nano-Al_2O_3 particle addition on grain structure evolution and mechanical behaviour of friction-stir-processed Al. Mater Sci Eng A, 2014. 602(0): p. 143–149
15. Al-Fadhalah K.J., Almazrouee A.I., and Aloraier A.S., Microstructure and mechanical properties of multi-pass friction stir processed aluminum alloy 6063. Materials & Design, 2014. 53(0): p. 550–560
16. Sato YS, Kokawa H, Enomoto M, Jogan S (1999) Microstructural evolution of 6063 aluminum during friction-stir welding. Metall Mater Trans A 30(9):2429–2437
17. Du Z, Tan MJ, Guo JF, Bi G, Wei J (2016) Fabrication of a new Al-Al_2O_3-CNTs composite using friction stir processing (FSP). Mater Sci Eng A 667:125–131
18. Takahara H, Tsujikawa M, Chung SW, Okawa Y, Higashi K, Oki S (2008) Optimization of welding condition for nonlinear friction stir welding. Mater Trans 49(6):1359–1364
19. Kwon Y, Saito N, Shigematsu I (2002) Friction stir process as a new manufacturing technique of ultrafine grained aluminum alloy. J Mater Sci Lett 21(19):1473–1476
20. Martin J.W., Micromechanisms in particle-hardened alloys. 1980: CUP Archive
21. Committee A.h., Properties and selection: nonferros alloys and special-purpose materials. 1991, Materials Park, OH: ASM International